Journal of Materials Chemistry A

Accepted Manuscript

This article can be cited before page numbers have been issued, to do this please use: P. Nayak, Q. Jiang, N. Kurra, U. Buttner, X. Wang and H. N. Alshareef, *J. Mater. Chem. A*, 2017, DOI: 10.1039/C7TA06236B.

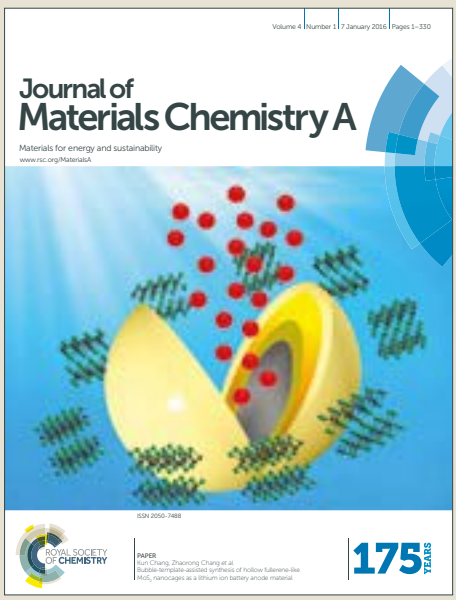

ROYAL SOCIETY OF CHEMISTRY

rsc.li/materials-a

View Article Online
DOI: 10.1039/C7TA06236B

Journal Name

ARTICLE

Monolithic Laser Scribed Graphene Scaffold with Atomic Layer Deposited Platinum for Hydrogen Evolution Reaction

Received 00th January 20xx,
Accepted 00th January 20xx

DOI: 10.1039/x0xx00000x

www.rsc.org/

Pranati Nayak,[1,2,⊥] Qiu Jiang,[1,⊥] Narendra Kurra,[1,⊥] Xianbin Wang,[1] Ulrich Buttner,[1] and Husam N. Alshareef[1*]

Three-dimensional (3D) electrode architectures for conformal deposition and effective use of catalyst is an emerging area with significant interest in electrocatalytic applications. In this study, we report the fabrication of monolithic, self-standing, 3D graphitic carbon scaffold with conformally deposited Pt by atomic layer deposition (ALD) as a hydrogen evolution reaction catalyst. Laser scribing is employed to transform polyimide into 3D porous graphitic carbon, which possesses good electronic conductivity and numerous edge plane sites. This laser scribed graphene (LSG) architecture makes it possible to fabricate monolithic electrocatalyst support without any binders or conductive additives. The synergistic effect between ALD of Pt on 3D network of LSG provides an avenue for minimal yet effective usage of Pt leading to an enhanced HER activity. This strategy establish a general approach for inexpensive and large scale HER device fabrication with minimum catalyst cost.

Introduction

The limited availability of traditional fossil fuels and the adverse environmental health issues resulting from their massive consumption make it essential in developing alternate clean and renewable energy sources.[1,2] Hydrogen is considered as the cleanest carbon-free molecular fuel and green energy carrier for various applications.[3,4] However, currently the commercial production of hydrogen primarily relies on the steam methane reforming route, which is being resourced mainly from fossil reserves. This technology seems to be unviable since it involves high energy (heat) input followed by substantial amount of CO_2 release as a by-product.[5,6] Interestingly, water splitting is an eco-friendly methodology for H_2 production, which can be realized via electrochemical, photochemical, and photoelectrochemical techniques. A significant amount of research has been directed towards electrochemical water splitting which is potentially green and renewable for hydrogen production without CO_2 emissions.[7] However, for efficient H_2 production, optimal design of the electrocatalysts is required to speed up the hydrogen evolution reaction (HER) kinetics.[8] To date, various noble metals and semiconductors have been used as catalysts for HER. Apparently, metallic platinum (Pt) remains as an unbeatable catalyst due to its unprecedented catalytic activity in liberating H_2 from a pair of protons and electrons at high reaction rates and low over potentials (η).[9,10] For scaled up applications, the prohibitive cost of Pt remains as the biggest obstacle to its use.

Researchers have identified two main strategies to cope with the expensive cost of Pt, including replacing or reducing Pt consumption to achieve sustainable H_2 production. Electrocatalysts based on transition metals such as Fe, Co, Ni, Mo and their molecular derivatives have been employed as alternatives to expensive Pt.[11,12] However, cycling stability of these catalysts was found to be mediocre as they are prone to corrosion by acid electrolyte. Transition metal dichalcogenides and carbides such as MoS_2 and Mo_2C have also shown excellent electrocatalytic activity towards HER. However, their poor electronic conductivity prevents their use for commercial device fabrication.[13] In this scenario, developing technology that will markedly minimize the Pt use and in parallel increase its utilization efficiency is a key step for the future 'hydrogen economy'. One strategy could be employing Pt at the atomic scale supported on high surface area conducting carbon architectures for its minimum and effective utilization. Design schemes like anchoring Pt on 1D carbon nanotubes (CNTs), 2D graphene, g-C_3N_4, porous carbon, hetero-atom doped graphene have been reported to improve the HER activity and long-term stability with minimal Pt usage.[14-16] However, these highly efficient electrocatalysts used under experimental framework have the form of fine powder. Hence, polymeric binders, surfactants and extra conductive additives are needed during slurry preparation to make the film intact and conductive.[17-21] These additives result in devices with poorly-controlled structures, plenty of dead volumes, and adverse sites that are unfavorable for electron conduction. Additionally, the use of solution processing (slurry making)

View Article Online
DOI: 10.1039/C7TA06236B

restacks the materials, which limits the electrochemical active surface area and blocks the active sites of electrocatalysts resulting in an increase in resistance to mass transfer.[22] Also, mass production of identical devices with high reproducibility in performance is still an issue. Therefore, fabricating a 3D self-standing, flexible, porous and conductive monolithic support is highly desirable for incorporating electrocatalysts into the 3D scaffolds, which resolves the above stated issues associated with the device fabrication of powder electrocatalysts. These 3D conductive networks provide high specific surface area, which facilitates the ion diffusion, catalyst-electrolyte interaction and finally the electron transport during electrocatalytic processes, thus improving the reaction kinetics and overall HER performance.

Atomic layer deposition (ALD) is a powerful tool for precisely controlled dispersal of catalyst on substrate, which prevents its agglomeration and promotes its effective utilization. ALD is capable of controlling thickness of Pt to the monolayer scale, resulting in excellent HER activity.[23] Recently, Saha et al., demonstrated the HER activity of Pt coated Mo_2C by ALD.[24] Katuri et al., have employed Pt coating over 3D polymeric hollow fiber membrane by ALD for recovery of both H_2 energy (through HER) and fresh water concurrently followed by waste-water treatment.[25]

In this study, we employ a direct-write laser technique to fabricate binder-free, monolithic, porous, conductive 3D interconnected network of 2D graphene sheets (henceforth referred to as laser scribed graphene or LSG) from commercial polyimide (PI). The self-standing scaffold is rich in edge plane sites but still functional enough to be wetted by the aqueous electrolytes. These flexible LSG electrodes were then conformally coated with Pt using ALD (Pt/LSG). The loading of Pt catalyst are precisely controlled by tuning the number of ALD cycles and we did a systematic study on its HER activity. The Pt/LSG electrodes show promising for the best utilization of catalyst with much less Pt loading signified by the high current density comparable to commercial Pt catalyst. Also a very good stability with high reproducibility is observed for Pt/LSG electrodes.

Results and Discussion

Figure 1a shows a schematic illustrating the fabrication of LSG electrodes on a PI sheet using laser scribing technique. It has been previously demonstrated that the energetic laser beam could transform insulating PI into conductive graphitic carbon that was employed as electrode for supercapacitors and electrochemical sensors.[26-27] X-Y translational movement of laser beam would allow scalable fabrication of graphitic carbon electrodes on a PI sheet in a desirable pattern. The intrinsic chemical inertness of the LSG scaffold may not be a good choice of electrocatalyst by itself. However, sensitization with metal catalyst could be a potential option, especially using a conformal deposition process that can effectively cover the 3D porous architecture of LSG (Fig. 1b and c). The morphology of as-obtained LSG and Pt/LSG using different number of ALD cycles was characterized using SEM. The morphology of LSG is seen to be porous with 3D perspective, abundant of edge-plane sites as shown in the SEM micrographs (see Fig. 1b projection and Electronic Supplementary Information, ESI, Fig. S1). In fact, the focused laser beam helps in carbonization and

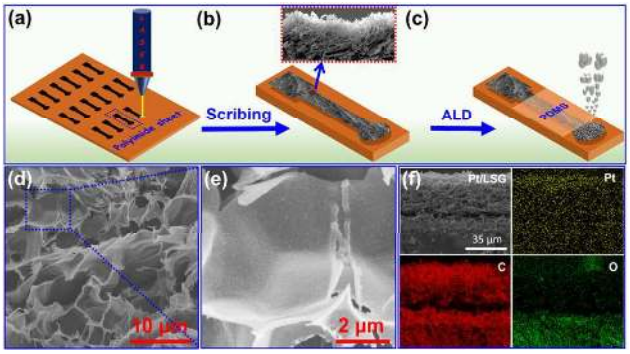

Fig. 1 Schematic illustrating the fabrication of LSG and Pt/LSG electrode patterns on PI sheet: (a) Fabrication of arrays of electrodes on PI sheet by laser scribing, (b) 3D view of the LSG electrode pattern. The projection displays vertical cross-sectional SEM image of a laser scribed PI sheet showing highly porous and protruded morphology of graphene, (c) selective passivation of electrode area by a PDMS and ALD of Pt selectively on the working electrode area, (d and e) SEM and high resolution SEM images of homogeneously coated ALD Pt over laser scribed graphene, (f) cross-sectional SEM micrograph and its corresponding elemental mapping images for C, O and Pt.

graphitization of PI surfaces due to very high local temperatures (>2500 °C).[26] Concurrently, the local availability of oxygen, and moisture in air during the graphitization process could burn-off some amount of carbon in the form of gaseous CO and CO_2, which makes LSG porous with less oxygen content. The intact 3D morphology offers high accessible electrochemical surface area, where as the edge-plane rich morphology of LSG pattern is anticipated to enhance catalytic activity.[27-28] Further, the catalytic activity of LSG was enhanced through surface coating of Pt by atomic layer deposition (ALD) (scheme shown in Fig. 1c). ALD is a unique technique because of its ability for conformal deposition of materials onto 3D architectures.[25] As LSG is highly porous, Pt deposition by ALD could ensure the uniform and homogeneous coverage of very thin Pt layer. Figures 1d-e illustrate the top-view SEM and high resolution SEM images of the Pt/LSG. The homogeneous deposition of Pt on LSG by ALD is confirmed by the SEM elemental mapping (shown in Fig. 1f and Fig. S2a-d). EDX spectrum shown in Figure S2e confirms the presence of Pt in the Pt/LSG sample). The loading of Pt on Pt/LSG electrodes was measured by calculating the weight difference after and before ALD cycles (shown in Fig. S2f). The relatively small mass loading (0.04 mg/cm^2 for 200 cycle ALD) of platinum on LSG compared to commercial Pt/C catalyst (0.5 mg/cm^2), which is nearly an order of magnitude lower mass loading compared to commercial Pt/C indicates the minimal yet effective usage of Pt by this ALD technique.

XRD and Raman spectroscopy were employed to investigate the structural characteristics of Pt/LSG electrodes. The XRD pattern (Fig. S3) of as prepared LSG confirms the graphitic

View Article Online
DOI: 10.1039/C7TA06236B

structure as evidenced by the presence of the typical C (002) peak at 2θ = 26.42º with corresponding interlayer spacing of ≈ 0.34 nm (d_{002}). The broad nature of C (002) peak depicts disorder in c-axis periodicity of 3D graphitic structure [29]. However, well-resolved peaks were obtained at 2θ = 35º and 70º for Pt/LSG

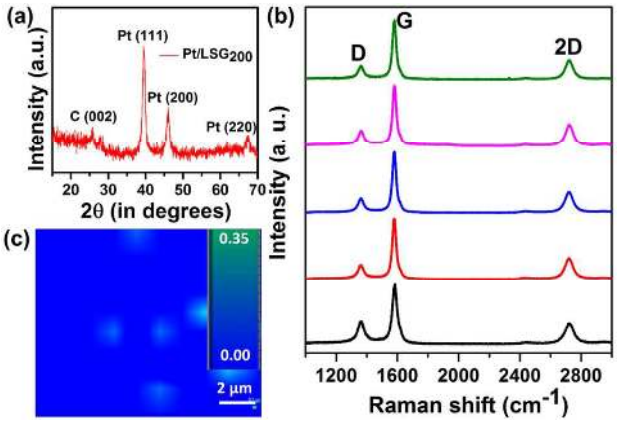

Fig. 2 (a) XRD pattern of the Pt/LSG electrodes, (b) Raman spectra at different regions on Pt/LSG showing uniform nature of graphitic carbon produced from the laser scribing process, and (c) I_D/I_G map of Pt/LSG over 10x10 µm area showing the uniform distribution of defects, indicating numerous available edge planes.

(Fig. 2a), which can be indexed to simple cubic structure of Pt (JCPDS No-87-0646).[30] The nature of graphitic carbon produced from laser scribing process was analyzed using Raman spectroscopy. Raman spectroscopy is a good structural characterization tool for carbon materials, especially graphitic type materials as these π-electrons can be polarized easily giving higher scattering cross-sections.[31] As shown in Fig. 2b, three dominant peaks are observed: D band (induced by bent sp^2 carbon bonds by breaking translational symmetry, essentially defect sites/functional groups), G band (corresponds to the E_{2g} vibration mode of graphitic carbon), and 2D band is due to periodicity and alignment of graphene layers along the c-axis.[31,32] Similar Raman signatures were observed at different regions of LSG sample. Typical D band position is observed at 1365.8 cm^{-1} with FWHM of 53.7 cm^{-1}, G band at 1583.5 cm^{-1} with FWHM of 36.3 cm^{-1} and 2D band at 2724.2 cm^{-1} with FWHM of 76.2 cm^{-1}. Though 2D band is seen as a single symmetric peak, its broadness up to 76 cm^{-1} is a clear indication of its turbostratic nature of graphene sheets in LSG.[33] The laser scribing process seems to trigger the depolymerization of PI, causing subsequent carbonization and graphitization, resulting in the formation of the graphitic domains. As this process is carried out under ambient conditions, availability of surplus amount of oxygen and water molecules in the surrounding environment under such high temperature conditions react with graphitic carbon releasing some of it in the form of CO and CO_2 gases. However, the non-uniform distribution of oxygen, water molecules and intense laser energy produces an intricate morphology of 3D porous graphitic carbon in this laser scribing process. The details of Raman spectra features are tabulated in Table S1 in the ESI. The typical I_D/I_G ratio for Pt/LSG is found to be in the range of 0.2 - 0.23, and corresponding graphitic crystallite size is of ~ 50 nm, estimated using the following equation.[34]

$L_a\,(nm) = 560/E^4_{laser}(I_D/I_G)^{-1}$ .....(1)

where E_{laser} is the laser excitation energy in eV.

As shown in Fig. 2c, the I_D/I_G map shows an average value of 0.21 (well in agreement with previous reports), and uniform distribution of defects, which could be beneficial for providing more electrochemical active sites and improving the catalytic activity.[26]

Electrochemical activity and durability

The electrocatalytic HER performance of as prepared LSG and Pt/LSG electrodes were compared by doing LSV at 5 mV/s in 0.5 M H_2SO_4 utilizing a conventional three-electrode set up consisting LSG as working electrodes, Pt wire as counter electrode, and Ag/AgCl (3 M KCl) as reference electrodes (Fig. 3a). To make a comparison, commercial Pt/C catalyst cathode (10 wt% on Vulcan XC-72R carbon black) was also tested under the same conditions. The commercial Pt/C catalysts were mixed with Nafion solution and drop-cast on glassy carbon electrode for HER tests (details discussed in ESI). The electrochemical polarization curves of LSG and Pt/LSG based electrodes are portrayed in Fig. 3b. The HER onset over potential of as prepared LSG electrode was determined to be ≈ 0.667 V, indicating little activity towards hydrogen evolution. However, Pt/LSG_{20} showed substantial decrease of onset potential to 0.188 V. Further, as the Pt content was increased by the number of ALD cycles, the onset potential of Pt/LSG electrodes gradually decreased. The specific activity for all samples was calculated from the polarization curves by normalizing the current with the geometric area of the electrodes. Further investigation of HER activity was done by fitting the linear region of the Tafel plot using the Tafel equation.[24]

$\eta = a + b \log |J|$..... (2)

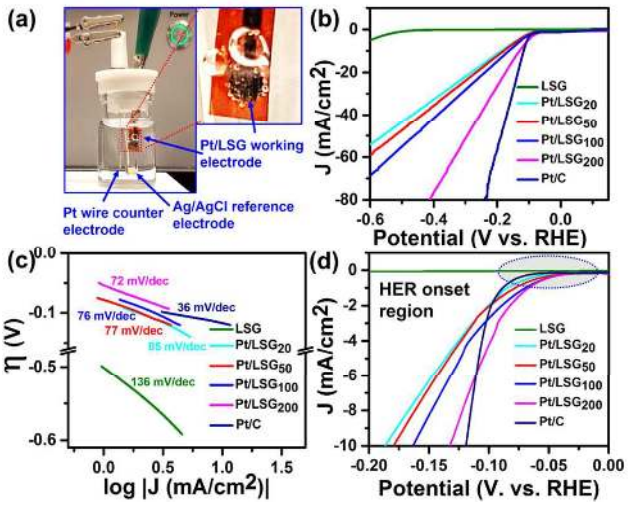

Fig. 3 Electrochemical performance of Pt/LSG electrodes compared to bare LSG and commercial Pt/C in 0.5 M H_2SO_4 electrolyte. (a) Digital

View Article Online
DOI: 10.1039/C7TA06236B

photograph showing 3 electrode system comprising LSG based electrode as working, Pt wire counter and Ag/AgCl as reference electrode. The photograph was taken when the cell turned on for 20 s. Inset showing H_2 bubble formation up on start of the LSV cycle, (b) LSV and (c) Tafel plots for Pt/LSG electrodes at varied number of ALD cycles compared to LSG and commercial Pt/C, (d) LSV showing HER onset region for LSG and Pt/LSG electrodes compared to commercial Pt/C.

where, η is the overpotential, J is the current density, b is the Tafel slope and 'a' is the intercept of the plot. The Tafel plots for each LSG and Pt/LSG electrodes were compared as shown in Fig. 3c. The Tafel slopes of Pt/C, LSG, Pt/LSG_{20}, Pt/LSG_{50}, Pt/LSG_{100} and Pt/LSG_{200} were found to be ≈ 36, 136, 85, 77, 76, and 72 mV/dec, respectively. It seems that Pt/LSG_{200} showed inferior activity towards HER over commercial Pt/C, however, the point to be noted here is based on self-standing nature of the Pt/LSG_{200} electrodes. Further, it can be improved by doping LSG electrodes by hetero-atom doping and engineering the architecture of LSG to achieve the HER activity matching that of commercial Pt/C, deserves future investigations.

The better performance of our Pt/LSG electrode toward HER may be attributed to the strong chemical/electronic coupling between ALD Pt and LSG sheets. In addition, the growth of highly dispersed Pt nanoparticles on the 3D network of LSG yields numerous available active catalytic sites for HER. The electronic coupling of highly dispersed ALD Pt to the underlying 3D network of LSG sheets with sufficient conductivity facilitates rapid electron transport. It was observed that the onset over-potential for HER remained more or less the same (i.e., between -0.03 and -0.05 V vs RHE) for the Pt/LSG electrodes prepared using different numbers of ALD cycles. However, at high HER current density (10 mA/cm^2), the over-potentials vary with the number of ALD Pt cycles. In contrast, the onset potential dramatically decreases to lower value after 20 Pt ALD cycles liberating more cathodic current (Fig. 3d, Table S2). With increased ALD cycles, the cathodic current density of the Pt/LSG_{200} electrode rose rapidly and approached that of commercial Pt/C.

The stability of the prepared Pt/LSG catalyst electrodes were further evaluated in acidic electrolyte. The electrodes were allowed to undergo LSV cycles continuously between −0.6 and 0.15 V in 0.5 M H_2SO_4 for 10,000 times, and finally the initial and final LSVs were compared, as shown in Fig. 4a. Note that the HER overpotential of Pt/LSG electrodes after 10,000 sweeps was almost the same as the initial overpotential. Also, similar J-V curve along with very negligible loss of cathodic current is observed after cycling test, thus demonstrating a very good stability of the Pt/LSG electrodes. In addition, the long-term stability of the Pt/LSG electrode was studied by extended electrolysis at fixed potentials in 0.5 M H_2SO_4 for a long time of 10 h (Fig. 4b). As an example, the stability of Pt/LSG_{200} electrode was tested because of its high HER activity and compared with bare LSG electrode. The catalytic current almost remained at -15 mA/cm^2 at −0.2 V (vs RHE) for Pt/LSG_{200} and -0.7 mA/cm^2 at -0.6 V for bare LSG electrodes, which reveals its excellent stability. It is worth mentioning that the hydrogen bubbles formed on the Pt/LSG_{200} electrode was vigorous (see Electronic Supplementary Information, ESI, video clip), which resulted noisy i-t data for Pt/LSG compared to bare LSG electrode. Thus, the prepared Pt/LSG electrode materials displayed not only very high HER activity but also showed excellent stability in acidic electrolyte medium. Since device reproducibility is a decisive factor, we tested five different electrodes prepared using different ALD cycles. A negligible variance in the onset potential

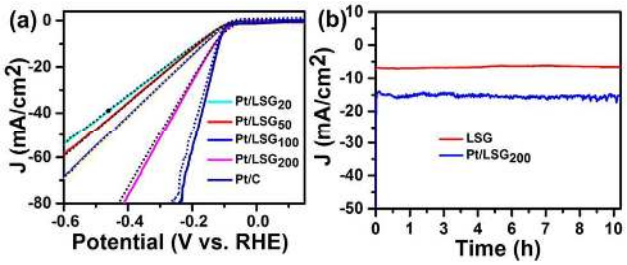

Fig. 4 (a) Comparison of LSV curves before and after stability measurements in 0.5 M H_2SO_4 (the dashed lines indicate the LSV recorded after 10,000 cycles, which is compared to 1st LSV cycle (corresponding solid line)), (b) amperometric i-t plot for LSG and Pt/LSG_{200} at a constant potential of -0.6 and -0.2 V respectively showing high stability of current density over a period of 10 h.

is observed, indicating very good reproducibility (shown in Fig. S4). The high HER activity, good stability and reproducibility of the Pt/LSG electrodes can be attributed to the combination of following factors: (i) the good electrical conductivity of binder-free self-standing LSG electrodes, which allows for effective charge transfer (ii) the high electrochemical active surface area of LSG, which facilitates the ion absorption and transport, and (iii) the synergistic effect between ALD Pt and 3D porous LSG, which plays an important role in the enhancement of HER activity with minimal Pt usage, and finally (iv) highly reproducible laser scribing and ALD processes.

Conclusion

In summary, direct laser scribing strategy was developed to fabricate self-standing, 3D network of graphene-like electrodes with conformal surface-coated Pt via atomic layer deposition for HER applications. These electrodes were found to be highly active for hydrogen evolution reaction in acidic medium. The synergistic effect between ALD Pt and 3D porous LSG play an important role in the enhancement of HER activity with minimal Pt usage, which is about one order of less loading compared to commercial Pt/C catalyst. In particular, the Pt/LSG_{200} electrode exhibits *the lowest over potential* (-131 mV) reported at a current density of -10 mA cm^{-2} in acidic media, which is very close to the benchmark Pt/C electrode (-118 mV, 10 wt% Pt catalyst). In addition, these electrodes exhibited long-term stability and good reproducibility in acidic media. Our 3D self-supporting electrode strategy, combined with ALD, opens a new pathway for scalable production efficient water-splitting electrodes.

Experimental Section

Reagents and Materials

View Article Online
DOI: 10.1039/C7TA06236B

Porous LSG electrodes were fabricated by laser scribing over commercial PI substrate (125 µm thickness). Trimethyl (methylcyclopentadienyl) platinum (IV) ($MeCpPtMe_3$) used as Pt precursor and sulphuric acid (H_2SO_4) were purchased from Sigma Aldrich. SYLGARD 184 silicone elastomer enclosing of base elastomer/curing Agent (Dow Corning) were mixed in a 10 (base):1 (curing agent) ratio by weight manually and was degassed by keeping under vacuum for 30 min in order to remove air bubbles prior to use as passivation layer on LSG electrodes. Conducting silver paint was procured from TED Pella, USA. The reagents used in this study were of analytical grade and were used as received. All stock solutions were prepared using deionized water (18.2 MΩ cm, Milli-Q Direct, Merck Millipore, and Nillerica, MA) without further purification.

Formation of laser scribed graphene scaffold

Laser scribing was performed by CO_2 Universal laser system (Universal X-660 laser cutter platform, λ = 1060 nm, pulse duration ~ 14 µs). The platform is equipped with translational X-Y control stage with varying scan rates from 0.7 to 23 inches/s. The power can be varied from 2.4 to 5.4 W with the pulses per inch (PPI) in the range of 1 to 1000. Laser PPI can be controlled by setting (100% corresponds to an absolute value of 1000 pulses per inch). For fabrication of LSG electrodes, the laser settings including peak power, speed, PPI and the z-distance between laser source and the sample were optimized to be 15%, 10% and 1000 and 2 mm, respectively. Computer controlled Corel draw software was employed to design the LSG electrode patterns on PI sheet. The laser beam size is roughly around 100 µm. Prior to use, the PI sheet was cleaned by rinsing with ethanol followed by water and then dried off by blowing nitrogen gas. All the electrode patterns were prepared under ambient conditions. Under these experimental conditions, the average thickness of the 3D porous LSG was found to be ~50 µm.

Atomic layer deposition of Pt

ALD of platinum on LSG electrodes was carried out using Oxford Instrument ALD system (FlexAL), which provides both thermal and remote plasma enhanced ALD configurations. Commercially available trimethyl(methylcyclopentadienyl) platinum(IV) ($Pt(MeCp)Me_3$, Sigma-Aldrich Ltd.) was used as platinum precursor and inductively coupled plasma (ICP) of oxygen was used as reactant. The temperature of precursor was maintained at 70 °C. $Pt(MeCp)Me_3$ vapor was carried into the process chamber through Ar bubbler gas at a flow rate of 150 sccm. The ALD process of platinum follows the standard deposition cycle sequence: First a pulse of Pt precursor vapor is introduced, followed by an Ar gas purge, then a pulse of oxygen plasma, followed by another Ar gas purge. A modification to the above mentioned standard ALD process was made by inserting a $Pt(MeCp)Me_3$ precursor soaking step between the platinum precursor pulse step and the following Ar gas purge step to prolong the dwell time of the precursor. This soaking step reduces the platinum precursor usage and helps to achieve a self-limited Pt growth on the LSG electrode surface. The deposition temperature was maintained at 200 °C. The following ALD process parameters were used: A precursor pulse time of 0.7 s, a soaking step of 3 s after the platinum precursor valve is closed, an oxygen plasma step of 3 s, and both ALD chamber purge steps after platinum dose and oxygen plasma of 3 s. Different platinum-loaded LSG substrates were prepared by varying the deposition cycles from 20 to 200. These prepared electrodes are henceforth referred to as Pt/LSG_{20}, Pt/LSG_{50}, Pt/LSG_{100}, and Pt/LSG_{200} in the manuscript.

Material Characterization

X-ray diffraction (XRD) patterns were measured using a Bruker diffractometer (D8 Advance) with Cu Kα radiation, λ = 1.5406 Å. The morphology and microstructure of the Pt/LSG based electrodes were characterized by high-resolution field emission scanning electron microscopy (FESEM) (Nova Nano 630, FEI). Energy-dispersive X-ray spectroscopy **(**EDX) column equipped with the SEM was used to do elemental analysis and also mapping to see the uniform coverage of Pt. Cross-sectional SEM was employed to measure the thickness of LSG and Pt/LSG films. Raman spectroscopy measurements were carried out on the samples using a micro-Raman spectrometer (LabRAM ARAMIS, Horiba-Jobin Yvon). Raman spectra were acquired with notch filters cutting at 100 cm^{-1} using a Cobalt laser (473 nm, 5 mW at source) with laser spot size of 1.5 µm. Raman mapping was done by continuous acquiring of spectra in a given scanning area (in this case 10x10 μm^2) with an adjacent spacing of 2 µm. Further, the acquired Raman data was processed to generate I_D/I_G map in order to know the defect distribution over a selected region of Pt/LSG.

Electrochemical characterization

The electrochemical HER activity of LSG based electrodes was evaluated using a three-electrode electrochemical cell comprising Pt wire counter electrode, Ag/AgCl (3M KCl) as reference electrode and LSG or Pt/LSG as working electrode using a CHI 6008 D electrochemical workstation (Austin, USA) at a scan rate of 5 mV/s. The physical area of the working electrode was defined (3 mm dia) using a thin-layer of polydimethylsiloxane (PDMS) which prevents contact of the electrolyte with the rest of the electrode area, as shown in ESI, Figure S1a. All the tests were performed in 0.5 M H_2SO_4 electrolyte in the potential range from 0 to -0.6 V. For stability study, the initial voltammogram was recorded at a scan rate of 5 mV/s followed by 10000 cycles at a scan rate of 100 mV/s, followed by linear sweep voltammetry (LSV) at 5 mV/s scan rate. Amperometric i-t measurement was carried out on LSG and Pt/LSG in order to study the stability of the current over time. All measurements were conducted under ambient conditions. The potential vs. Ag/AgCl was converted to reversible hydrogen electrode (RHE) using the Nernst equation: $E_{RHE} = E_{Ag/AgCl} + 0.059\ pH + E^{o}_{Ag/AgCl}$, for 0.5 M H_2SO_4, $E_{RHE} = E_{Ag/AgCl} + 0.21$ V.

Acknowledgements

Research reported in this publication is supported by funding from King Abdullah University of Science and Technology (KAUST), Saudi Arabia. Dr. P. Nayak would like to thank DST (Government of India) for the Inspire Faculty Award (Grant No. 04/2015/002660).

View Article Online
DOI: 10.1039/C7TA06236B

Notes and references

[1]Materials Science and Engineering, Physical Sciences & Engineering Division, King Abdullah University of Science and Technology (KAUST), Thuwal, 23955-6900, Saudi Arabia
[2]Electrodics and Electrocatalysis (EEC) Biosensor Division, CSIR-Central Electrochemical Research Institute (CSIR-CECRI), Karaikudi, Tamilnadu, 630006, India
[⊥] These authors contributed equally to the work
*Corresponding author: Husam Alshareef
E-mail: husam.alshareef@kaust.edu.sa

[†]Electronic Supplementary Information (ESI) available: [details of any supplementary information available should be included here]. See DOI: 10.1039/x0xx00000x

Fig. S1 (a) Digital photograph of a fully assembled LSG HER electrode scaffold, (b) Top-view SEM micrograph of LSG showing rich in edge plane sites, (c) Cross-sectional view of electrode showing its 3D porous nature and corresponding EDAX maps for C and O elements are shown.

Fig. S2 (a) Top-view SEM micrograph of Pt/LSG_{200} electrode showing it is rich in edge plane sites and having ALD Pt on surface, (b) corresponding elemental mapping of C K and (c) Pt M on Pt/LSG_{200} surface, (d) high magnification SEM micrograph of Pt/LSG_{200} showing surface coated Pt, (e) EDAX spectrum and (f) plot of mass loading of Pt on LSG after 100 and 200 ALD cycles.

Fig. S3 XRD pattern of as prepared LSG

Fig. S4 LSV showing HER onset region for five different Pt/LSG_{200} electrodes at 5 mV/s scan rate in 0.5 M H_2SO_4.

Table S1. Raman spectra analysis of Pt/LSG.

Table S2. Comparison of HER performance of LSG and Pt/LSG based electrodes

References

1 M. S. Dresselhaus and I. L. Thomas, *Nature*, 2001, **414**, 332.
2 J. A. Turner, *Science,* 1999, **285**, 687.
3 J. A. Turner, *Science,* 2004, **305**, 972.
4 Y. Jiao, Y. Zheng, M. Jaroniec and S. Z. Qiao, *Chem. Soc. Rev.,* 2015, 44, 2060.
5 S. Chu and A. Majumdar, *Nature*, 2012, **488**, 294.
6 N. Armaroli and V. Balzani, *Angew Chem. Int. Ed. Engl.,* 2007, **46**, 52.
7 T. Abbasi and S. A. Abbasi, *Renew. Sustainable Energy Rev.,* 2011, **15**, 3034.
8 M. Li, Q. Ma, W. Zi, X. Liu, X. Zhu and S. Liu, *Sci.Adv.,* 2015, **1**, 1400268.
9 W. Sheng, Z. Zhuang, M. Gao, J. Zheng, J. G. Chen and Y. Yan, *Nat. Commun.,* 2015, **6**, 5848.
10 J. Zheng, W. Sheng, Z. Zhuang, B. Xu and Y. Yan, *Sci. Adv.*, 2016, **2**, 1501602.
11 S. E. Moradi, *Chem. Biochem. Eng. Q.*, 2016, **30**, 1.
12 D. Jasion, J. M. Barforoush, Q. Qiao, Y. Zhu, S. Ren and K. C. Leonard, *ACS Catal.,* 2015, **5**, 6653.
13 T. Brulle, A. Denisenko, H. Sternschulte and U. Stimming, *Phys. Chem. Chem. Phys.,* 2011, **13**, 12883.
14 Y. Ito, W. Cong, T. Fujita, Z. Tang and M. Chen, *Angew. Chem. Int. Ed. Engl.,* 2015, **54**, 2131.
15 Y. Y. Chen, Y. Zhang, W. J. Jiang, X. Zhang, Z. Dai, L. J. Wan and J. S. Hu, *ACS Nano*, 2016, **10**, 8851.
16 Y. Zheng, Y. Jiao, L. H. Li, T. Xing, Y. Chen, M. Jaroniec and S. Z. Qiao, *ACS Nano,* 2016, **10**, 5290.
17 D. H. Youn, S. Han, J. Y. Kim, J. Y. Kim, H. Park, S. H. Choi and J. S. Lee, *ACS Nano,* 2014, **8**, 5164.
18 H. Dong, C. Liu, H. Ye, L. Hu, B. Fugetsu, W. Dai, Y. Cao, X. Qi, H. Lu and X. Zhang, *Sci. Rep.,* 2015, **5**, 17542.
19 Y. Jia, L. Zhang, A. Du, G. Gao, J. Chen, X. Yan, C. L. Brown and X. Yao, *Adv. Mater.,* 2016, **28**, 9532.
20 S. Mao, G. Lu and J. Chen, *Nanoscale*, 2015, **7**, 6924.
21 P. Nayak, B. Anbarasan, S. Ramaprabhu, *J. Phys. Chem. C,* 2013, **117**, 13202.
22 Y. Wang, Y. Wu, Y. Huang, F. Zhang, X. Yang, Y. Ma and Y. Chen, *J. Phys. Chem. C,* 2011, **115**, 23192.
23 N. P. Dasgupta, C. Liu, S. Andrews, F. B. Prinz and P. Yang, *J. Am. Chem. Soc.,* **135**, 2013, 12932.
24 S. Saha, B. Martin, B. Leonard and D. Li, *J. Mater. Chem. A,* 2016, **4**, 9253.
25 K. P. Katuri, N. M. Bettahalli, X. Wang, G. Matar, S. Chisca, S. P. Nunes and P. E. Saikaly, *Adv. Mater.,* 2016, **28**, 9504.
26 J. Lin, Z. Peng, Y. Liu, F. Ruiz-Zepeda, R. Ye, E. L. Samuel, M. J. Yacaman, B. I. Yakobson, J. M. Tour, *Nat. Commun.*, 2014, **5**, 5714.
27 P. Nayak, N. Kurra, C. Xia and H. N. Alshareef, *Adv. Electron. Mater.,* 2016, **2**, 1600185.
28 C. E. Banks, T. J. Davies, G. G. Wildgoose and R. G. Compton, *Chem. Commun.*, 2005, **7**, 829.
29 P. Nayak and S. Ramaprabhu, *J. Phys. Chem. C,* 2015, **119**, 2917.
30 M. Baro, P. Nayak, T. T. Baby and S. Ramaprabhu, *J. Mater. Chem. A,* 2013, **1**, 482.
31 A. C. Ferrari and J. Robertson, *Phys. Rev. B,* 2000, **61**, 14095.
32 N. Kurra, A. A. Sagade and G. U. Kulkarni, *Adv. Funct. Mater.,* 2011, **21**, 3836.
33 N. Kurra and G. U. Kulkarni, *Lab Chip,* 2013, **13**, 2866.
34 M. A. Pimenta, G. Dresselhaus, M. S. Dresselhaus, L. G. Cancado, A. Jorio and R. Saito, *Phys. Chem. Chem. Phys.,* 2007, **9**, 1276.

View Article Online
DOI: 10.1039/C7TA06236B

Graphic Art

Atomic layer deposition (ALD) of Pt over monolithic 3D porous, laser scribed graphene scaffolds forms an efficient electrocatalyst for hydrogen evolution reaction.